# On the production of the six-quark $H$ dibaryon in the $(K^-,K^+)$ reaction

A. T. M. Aerts and C. B. Dover
*Brookhaven National Laboratory, Upton, New York 11973*
(Received 21 March 1983)

We investigate several ways of producing the stable doubly strange six-quark dibaryon $H$ predicted by the MIT bag model. Various kinematical and dynamical arguments indicate that the $(K^-,K^+)$ double-strangeness-exchange reaction on nuclear targets affords the best chance for observing the $H$. Cross sections for the prototype reaction $^3\mathrm{He}(K^-,K^+n)H$ are calculated, using empirical data on the reaction $K^-p\to K^+\Xi^-$ as input, as well as an oscillator model for the quark-fusion process $\Xi^-p\to H$. The spectrum for the quasielastic process $^3\mathrm{He}(K^-,K^+)n\Xi^-p$ is also calculated. For coincidence experiments involving both $K^+$ and neutron detection at forward angles, the cross section for $H$ production ranges from 10—30 nb/sr$^2$ for $K^-$ beam momenta between 1.4 and 2.2 GeV/$c$. If the $H$ lies below the $\Lambda\Lambda$ threshold, it can be nicely separated from the $K^+$ quasielastic background, although $\pi^+$'s misidentified as $K^+$'s can be a problem for certain $H$ masses. If only the $K^+$ is detected, the separation of the $H$ signal ($\approx 0.5\ \mu$b/sr) from the quasielastic background can be achieved through a careful measurement of the $K^+$ momentum spectrum. We assess the effects on our results of the rapid momentum dependence in the $K^-p\to K^+\Xi^-$ reaction, as well as short-range correlations in the $^3$He wave function.

## I. INTRODUCTION

In the naive quark model, the low-lying baryons and mesons are thought of as composites of three quarks ($Q^3$) or a quark and an antiquark ($Q\bar{Q}$), respectively. In addition to these configurations, phenomenological quark models (for instance, the MIT bag model[1]) predict the existence of other, generally more massive states of structure $Q^m\bar{Q}^n$, with $m+n\geq 4$. As examples, we mention the $Q^2\bar{Q}^2$ "baryonium" configurations,[2] the "$Z^*$ resonances" ($Q^4\bar{Q}$) of strangeness $S=+1$ (see Ref. 3), and the $Q^6$ dibaryons. The latter case has been of intense interest: evidence for dibaryon resonances in nucleon-nucleon ($NN$) scattering has been reviewed in Ref. 4, and the peak (or peaks) near 2129 MeV in the $\Lambda p$ invariant-mass spectrum[5] (as seen in $K^-d\to\pi^-\Lambda p$) may offer another candidate. The problem in interpreting such structures as six-quark bag states (with $S=0$ or $-1$) is that each lies well above the threshold for decay into two baryons. It has proven difficult to disentangle quark aspects from ordinary hadronic mechanisms (coupling of $NN$ to the $N\Delta$ channel, for instance) when the effects due to the latter are strong. Treatments of the $NN\leftrightarrow N\Delta$ and $\Lambda N\leftrightarrow\Sigma N$ problems have been offered in Refs. 6 and 7, respectively; these do not involve explicit consideration of quark degrees of freedom.

Among the spectrum of six-quark bag states,[8—11] the $S=-2$ sector plays a special role. Indeed, only a six-quark system containing two up ($u$), two down ($d$), and two strange ($s$) quarks can exist in an SU(3)-flavor singlet with spin zero, a configuration which takes maximum advantage of the attraction due to the color-magnetic interactions[12] of quantum chromodynamics (QCD). It is possible that such a six-quark system might be *stable* with respect to strong decay into all baryon-baryon channels (the lowest-lying of which is $\Lambda\Lambda$). This was first noted by Jaffe,[8] who predicted that the ($uuddss$) state with spin-parity $J^\pi=0^+$, isospin $I=0$, which he called the $H$ particle, would have a mass $m_H\approx 2150$ MeV, some 80 MeV below the $\Lambda\Lambda$ threshold. More recently, several other calculations of the $H$ mass have appeared, which include center-of-mass[13] or pionic-cloud[14] corrections within the context of the MIT bag model.[1,8] These calculations give less binding for the $H$ than obtained by Jaffe,[8] but the $H$ remains close to or below the $\Lambda\Lambda$ threshold. Independent of calculational details, one expects that an object with the quantum numbers of the $H$, which maximizes the color-magnetic attraction between the quarks,[12] is the most likely candidate for a stable six-quark bag state.

If the $H$ exists and is indeed stable, it will be a unique object in multiquark spectroscopy ($n>3$). In ordinary potential models involving boson exchange, *deeply bound* states in the $\Lambda\Lambda$, $\Xi N$, and $\Sigma\Sigma$ channels, which can share the quantum numbers of the $H$, are not expected. The $H$ is to be thought of as a genuine six-quark object, with all the quarks in one bag, rather than a weakly bound "quasimolecule" such as the deuteron, where the two rather well separated three-quark bags retain much of their identity.

The $H$ has been searched[15] for the reaction $p+p\to K^++K^++H$ at the Brookhaven Alternating Gradient Synchrotron. The $H$ was not seen, but the upper limit of 40—50 nb for the cross section (mass range $2.1<m_H<2.23$ GeV) is too crude to rule out its existence. In this paper, we argue that a more natural way to produce the $H$ is to utilize an $S=-1$ incident beam ($K^-$ or $\bar{K}^0$), and to transfer two units of strangeness to a nuclear system (exit particle is $K^+$ or $K^0$ with $S=+1$), which then recoils with $S=-2$. By bringing in one unit of strangeness, one obviates the need for *double* associated production, as in $p+p\to K^++K^++H$. Strangeness-exchange reactions (both single and double) have considerably larger cross sections than associated-production processes, and are thus intrinsically more favorable for $H$ production.

The outline of the paper is as follows. In Sec. II, we review the phenomenology of the $H$ particle. The formalism appropriate to the calculation of the $(\bar{K},K)$ cross sec-

 

tions on a $^3$He target is outlined in Sec. III. We obtain both the $H$ production cross section and the "quasielastic" background due to continuum $\Xi$-nucleon pairs. The calculation requires a model for the elementary two-body process $\bar{K}N \to K\Xi$, the $^3$He wave function, and the vertex $\Gamma$ for the fusion of two three-quark bags ($\Xi$ and $N$) into the six quark $H$. These ingredients are also discussed in Sec. III.

Our numerical results for the prototype reaction $^3\mathrm{He}(K^-,K^+)Hn$ are examined in Sec. IV. We focus on two types of measurements, one in which only the $K^+$ is detected, and a second in which the $K^+$ and neutron are measured in coincidence. In the former case, $H$ production is characterized by a sharp peak in the $K^+$ momentum spectrum. If the $H$ lies below the $\Lambda\Lambda$ threshold, this peak is clearly separated from a broader "quasielastic" peak due to the process $^3\mathrm{He}(K^-,K^+)\Xi^-pn$, involving a continuum four-body final state. For the coincidence experiment, a stable $H$ shows up as an isolated peak in the missing-mass spectrum, below the onset of the continuum background. The calculated cross sections for $H$ production are at a level which may be accessible with present kaon-beam intensities, although the existence of a "kaon factory" would greatly enhance the prospects for such double-strangeness-exchange experiments.

In Sec. V, we discuss other potential sources of background, namely, $\pi^+$ mesons from reactions such as $^3\mathrm{He}(K^-,\pi^+)\Sigma^-pn$. Such processes can produce copious numbers of pions in the same momentum range as the $K^+$'s from $H$ production. Experimentally, one must be able to clearly distinguish $\pi^+$'s and $K^+$'s around 1.4—1.5 GeV/$c$ in order to detect the $H$ signal.

A brief summary is provided in Sec. VI.

## II. DIBARYONS IN THE QUARK MODEL: THE $H$

In the MIT bag model,[1] the color gauge theory of quarks and gluons (QCD) has been adapted to conventional meson and baryon spectroscopies. The parameters of the model have been determined by a fit to the spectrum of low-lying $Q\bar{Q}$ mesons and $Q^3$ baryons. Without additional parameters, the model may be extended to any multiquark color singlet system $Q^n\bar{Q}^m$, with $n+m>3$. Jaffe[8] first pointed out that the MIT bag model predicts for the $Q^6$ system several relatively light $S=-2$ dibaryons, one of which (the $H$), with $J^\pi=0^+$, $I=0$ could be stable against strong decay. Later, the Nijmegen group[9–11] explored the $Q^6$ spectrum for all allowed values of hypercharge, and again found the $H$ as the only candidate for a stable dibaryon.

These earlier calculations of the $H$ mass concentrated on the color-magnetic interactions[8] between the quarks, the importance of which is illustrated by the size of the $N-\Delta$ splitting. The color-magnetic interaction term in the MIT bag model has the form

$$H_m = -\frac{\alpha_c}{R}\sum_{i<j} M(m_iR,m_jR)(F\sigma)_i(F\sigma)_j \ , \tag{2.1}$$

where $\alpha_c$ is the QCD coupling constant, $R$ is the bag radius, and $m_i$ is the mass of quark $i$. $F_i$ and $\sigma_i$ are the color and spin operators of quark $i$. If we ignore differences in the quark masses between nonstrange and strange quarks for the moment, we see that $H_m$ is proportional to

$$A = -\sum_{i<j}(F\sigma)_i(F\sigma)_j \tag{2.2}$$

$$= \tfrac{1}{4}N(N-10)+\tfrac{1}{3}S(S+1)+\tfrac{1}{2}f_c{}^2+f_F{}^2 \tag{2.3}$$

for systems composed of $u$, $d$, and $s$ quarks; $f^2$ denotes the eigenvalue of the quadratic Casimir operator[11] for SU(3). Clearly, a hadron which is a color, flavor, and spin singlet ($f_c{}^2=f_F{}^2=S=0$), such as the $H$, has the largest color-magnetic attraction.

To see in more detail which parts of the $H$ wave function contribute most to this attraction, we decompose it into $Q^4\otimes Q^2$ components in the shorthand notation $Q^n(\underline{f},s,c)$:

$$Q^6(\underline{1},0,1)=(\tfrac{1}{10})^{1/2}Q^4(\underline{6}^*,0,6^*)\otimes Q^2(\underline{6},0,6)+(\tfrac{3}{10})^{1/2}Q^4(\underline{3},1,6^*)\otimes Q^2(\underline{3}^*,1,6)$$
$$+(\tfrac{3}{10})^{1/2}Q^4(\underline{6}^*,1,3)\otimes Q^2(6,1,3^*)+(\tfrac{3}{10})^{1/2}Q^4(\underline{3},0,3)\otimes Q^2(\underline{3}^*,0,3^*) \ . \tag{2.4}$$

This gives, with $\mu=m_sR$ ($m_u=m_d=0$),

$$\langle H\,|\,H_m\,|\,H\rangle = -\frac{\alpha_c}{4R}[5M(0,0)+22M(0,\mu) - 3M(\mu,\mu)] \ . \tag{2.5}$$

The color-magnetic interaction is attractive when both color and spin wave functions have the same symmetry, and is repulsive (but half as strong) otherwise. The Pauli principal requires the former configuration to pair up with the antisymmetric flavor representation, which is why the effect of the strange-quark—nonstrange-quark interactions is so large. Note that the presence of color creates a fundamental difference from the nuclear-physics analog, the $\alpha$ particle, where like particles are paired into spin singlets, and similarly with the electromagnetic analog, the Cooper pair. Using Eq. (2.5), one arrives at a mass $m_H=2150$ MeV.

In addition to the color-magnetic interaction, one should also consider corrections to the $Q^6$ spectrum due to spurious center-of-mass motion[13] or the possibility of a pion cloud around the bag.[14] Calculations which include these latter effects yield less binding for the $H$ than the earlier estimates[8–11]; predictions for the mass $m_H$ of the $H$ dibaryon are collected in Table I. Note that the correct method for including c.m. corrections in the bag model is still far from established; a repulsive shift of 100 MeV for the $H$ mass was obtained by Liu and Wong[13] in an admittedly *ad hoc* fashion, and should be considered only as a rough estimate of the c.m. correction. The calculations of Mulders and Thomas[14] still use a spherical and static bag, treating the pion field as a perturbation to avoid collapse of the bag. Inclusion of the pion field leads to substantial changes in the bag constants and the QCD coupling constant $\alpha_c$, in order to preserve the fit to ordinary meson and baryon spectroscopy. The $H$ becomes less bound with respect to the $\Lambda\Lambda$ threshold for two main reasons[14]: (i) $\alpha_c$

TABLE I. Estimates of the $H$ mass. Note that $2m_\Lambda \approx 2231$ MeV is the strong decay threshold.

| Reference | c.m. correction included? | Pion cloud? | $m_H$ (MeV) |
|---|---|---|---|
| Jaffe[8] | No | No | 2150 |
| Nijmegen[9–11] | No | No | 2200 |
| Liu and Wong[13] | Yes | No | 2240 |
| Mulders and Thomas[14] | No | Yes | 2220–2230 |

is reduced, leading to less color-magnetic attraction for the $H$; (ii) the self-energy due to the pion cloud, which has the form $E_\pi = -C/pR^3$, contributes about $-130$ MeV to the mass of the $\Lambda$. The $H$, which is assumed[14] to have a radius about 20% larger than that of the $\Lambda$, and a coefficient $C_H = 54$ less than $2C_\Lambda = 72$, receives only $-110$ MeV from its pion cloud. Clearly, these estimates are rather qualitative, so one should not take the results in Table I too seriously.

If the $H$ is stable, and relatively deeply bound (say 25 MeV), it cannot be confused with a deuteronlike object bound weakly by ordinary meson-exchange forces. To exhibit the two-baryon content of the $H$, we write its wave function in terms of $Q^3 \otimes Q^3$ components[16–18]

$$|H\rangle = (\tfrac{4}{5})^{1/2} |8_c \otimes 8_c\rangle + (\tfrac{1}{10})^{1/2} |\Xi N\rangle_{I=0} - (\tfrac{1}{40})^{1/2} |\Lambda\Lambda\rangle + (\tfrac{3}{40})^{1/2} |\Sigma\Sigma\rangle_{I=0} . \quad (2.6)$$

Note that 80% of the time, the $H$ falls apart *virtually* into two *color-octet* ($8_c$) three-quark systems.

Using the $\Lambda\Lambda$, $\Sigma\Sigma$, and $\Xi N$ meson-exchange potentials of the Nijmegen group,[19] we have found that no two-body bound states with $S = -2$ are expected. These models[19] incorporate SU(3) symmetry for coupling constants, and break this symmetry by using physical values for meson and baryon masses in recoil corrections to the static limit. A recent approach[20] using a quark-pairing mechanism to arrive at a one-boson-exchange model yields a somewhat different result. Here, lightly bound (1–2 MeV) $\Lambda\Lambda(^1S_0)$ and $\Xi N$ ($^3S_1$) states *may* occur; the $\Lambda\Lambda$ state shares the quantum numbers of the $H$. This model,[20] however, does not yield as high quality a fit to $NN$ and $YN$ data as that of Ref. 19. In any reasonable one-boson-exchange model, there is no mechanism for producing a *deeply bound* (tens of MeV) state with $S = -2$. This can occur only for six quarks in one bag. Note that in the boson models, the $\Lambda\Lambda$ potential is *repulsive* at short distances ($\omega$ exchange) and the long-ranged attractive pion-exchange term, which is mostly responsible for binding the deuteron, is essentially absent (except for charge-symmetry-breaking effects). Some intermediate-range attraction due to scalar ($\epsilon$) exchange remains, but this is not sufficient to produce deep $\Lambda\Lambda$ binding.

The masses in Table I refer to six-quark "primitives," i.e., poles in the $P$ matrix of Jaffe and Low.[21] The coupling of the primitives to the allowable baryon-baryon channels must be included before we identify $m_H$ with the physically observable mass of the $H$ (i.e., an $S$-matrix pole). The $S$-matrix pole corresponding to the $H$ generally lies *below* the $P$-matrix pole; Badalyan and Simonov[22] have estimated a downward shift of 15–30 MeV, but included only the coupling to the $\Lambda\Lambda$ channel. Soldate[22] has also included the $\Xi N$ and $\Sigma\Sigma$ channels, and finds a much larger shift, of order 100 MeV. Taking this shift into account, all mass values in Table I will yield $S$-matrix poles below the $\Lambda\Lambda$ threshold. In our calculations, $m_H$ refers to the $S$-matrix pole. The particular $P$-matrix parametrization of Badalyan and Simonov[22] predicts $\Lambda\Lambda$ phase shifts which differ markedly from those we have obtained using the boson-exchange model of Ref. 19. However, the $S$-matrix pole for the $H$ lies below the $P$-matrix pole for a wide class of parametrizations of the $P$ matrix.

An important ingredient in our calculations consists of the virtual dissociation amplitudes of the $H$ into various baryon-baryon channels, obtained from Eq. (2.6). For the case of the $(K^-,K^+)$ reaction, we need the $\Xi^- p \to H$ overlap vertex $\Gamma$. From Eq. (2.6), we see that the color-spin-flavor recoupling part of $\Gamma$ is

$$\Gamma_0 = \sqrt{1/20} \text{ for } \Xi^- p \to H \quad (2.7)$$

since $\Xi^- p$ has amplitude $\sqrt{1/2}$ for the $I=0$ state. Here we assume that the $\Xi^- p$ pair is prepared in the spin-singlet state. This will be the case if we consider the process $K^- + (pp) \to K^+ + (\Xi^- p)$ for $\theta_{K^+} = 0°$; here spin flip is absent and the diproton is automatically in the singlet state for $L=0$, due to the Pauli principle. Thus, antisymmetrization of the $pp$ pair in the nucleus leads to an enhancement of $\sqrt{2}$ in the amplitude for $H$ production, and leads to an effective value $\Gamma_0 = \sqrt{1/10}$, which we use later. Note that $\Gamma_0$ is maximal for the sequential production of an $H$ on a *bound* diproton ($L=0$ as well as $S=0$): $K^- + (pp)^1S_0 \to K^+ + (\Xi^- p)$ followed by $\Xi^- p \to H$. For $p + p \to K^+ + K^+ + H$, on the other hand, one expects the dominant process to be $p \to K^+ \Lambda$ dissociation (twice) followed by $\Lambda\Lambda \to H$ recombination. Here the continuum $pp$ system at high relative momentum has only a $\frac{1}{4}$ probability of being in the spin-singlet state, and this factor also prevails for the $\Lambda\Lambda$ system. Combined with the smaller amplitude for $|\Lambda\Lambda\rangle$ compared to $|\Xi N\rangle$ in Eq. (2.3), we find that $H$ production via *bound* diprotons is favored over production in $pp$ collisions by a factor of 16 from the spin-flavor-color factors alone. Note that $H$ production on deuterium (or bound $np$ pairs with spin one and isospin zero) is also unfavorable: the reaction $K^- d \to K^+ (\Xi^- n)_{I=1}$ produces a $\Xi N$ pair of the wrong isospin to become an $H$, while $K^- d \to K^0 (\Xi^- p)_{S=1}$ with the $K^0$ at 0° leads to the wrong spin. These simple considerations indicate that a bound diproton is the optimal "target" for making an $H$. The lightest bound nucleus containing a diproton is $^3$He, so we adopt $^3\text{He}(K^-,K^+)Hn$ as our prototype reaction for study. This reaction also has the advantage of having a simple three-body final state, so if one is able to measure the $K^+$ and neutron in coincidence, the resulting "missing-mass" spectrum should display a sharp peak at the $H$ mass (the width of which is just the experimental resolution, since the $H$ decays weakly).

## III. FORMALISM

The cross section for the prototype reaction

$$K^- + {}^3\text{He} \to K^+ + n + H , \quad (3.1)$$

integrated over all final states, can be written in the usual invariant way (e.g., Pilkuhn[23]) as

$$\sigma=\frac{1}{(2\pi)^5}\int\frac{d^3k'}{2E_{k'}}\int\frac{d^3p_n}{2E_n}\int\frac{d^3p_H}{2E_H}\delta^{(4)}(P-k'-p_n-p_H)\,|M^{(3)}|^2/2\lambda^{1/2}(s,m_{\mathrm{He}}{}^2,m_K{}^2)\ . \tag{3.2}$$

Here $k'=(\vec{k}\,',E_{k'})$, $p_n=(\vec{p}_n,E_n)$, and $p_H=(\vec{p}_H,E_H)$ are the four-momenta of the outgoing kaon, neutron, and $H$ dibaryon, respectively, with $E_{k'}=\{k'^2+m_k{}^2\}^{1/2}$, etc. Further, $s$ is the total invariant mass squared of the initial and final states,

$$P=(\vec{k}_L,m_{\mathrm{He}}+(k_L{}^2+m_K{}^2)^{1/2})\ ,$$

and

$$\lambda(a,b,c)=a^2+b^2+c^2-2(ab+bc+ca)$$

is the usual triangle function.[23] Equation (3.2) corresponds to normalizing the plane waves according to

$$\langle\vec{p}\,|\,\vec{p}\,'\rangle=2E(2\pi)^3\delta^{(3)}(\vec{p}-\vec{p}\,')\ .$$

Various differential cross sections are obtained by removing one or two of the three-momentum integrations in Eq. (3.2). These cross sections are computed in the $K^-+{}^3$He laboratory frame.

The invariant matrix element $M^{(3)}$ corresponds to the conversion of the initial diproton pair in $^3$He into the $H$ dibaryon via the $(K^-,K^+)$ process. In lowest order, this process is shown in the top half of Fig. 1. The analogous conversion of an $n$-$p$ pair into the $H$ via $(K^-,K^0)$ is shown in the lower part of the figure. The first step in this conversion is $\Xi^-$ production via the $K^-p\to K^+\Xi^-$ reaction, with amplitude $f$ defined in Eq. (3.6), followed by $\Xi^-p$ fusion into the $H$ through the vertex $\Gamma$. For the process of Fig. 1, we find an amplitude

$$M^{(3)}=(2E_H2M_{\mathrm{He}}2E_n)^{1/2}\int\frac{d^3k_\rho}{(2\pi)^3}\psi_{\mathrm{He}}(\vec{k}_\rho,\vec{k}_\lambda)T(\vec{k}_L,\vec{p}\,';\vec{k}\,',\vec{k}_\Xi)\Gamma(\vec{k}_\Xi-\vec{k}_p)/(2E_{p'}2E_\Xi)^{1/2}\ , \tag{3.3}$$

where $\psi_{\mathrm{He}}$ is the internal wave function of the $^3$He target and $T$ is the dimensionless amplitude corresponding to the $K^-p\to K^+\Xi^-$ reaction [see Eq. (3.6)]. The relevant momenta are defined by

$$\begin{aligned}\vec{k}_\rho&=-(2\vec{k}_p+\vec{p}_n)/\sqrt{2}\ ,\\ \vec{k}_\lambda&=-\sqrt{3/2}\vec{p}_n\ ,\\ \vec{p}\,'&=-\vec{k}_p-\vec{p}_n\ ,\\ \vec{k}_\Xi&=\vec{k}_H-\vec{k}_p\ .\end{aligned} \tag{3.4}$$

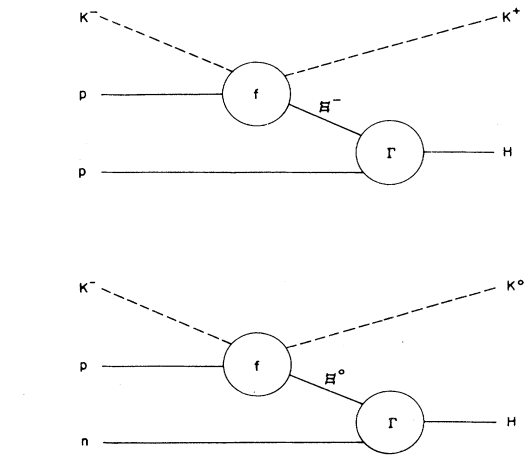


FIG. 1. Lowest-order processes for $H$ production on a diproton pair via the $(K^-,K^+)$ reaction (upper part) or on a neutron-proton pair in the $(K^-,K^0)$ reaction (lower part). The amplitude for the two-body transitions $K^-p\to K^+\Xi^-$ or $K^0\Xi^0$ is denoted by $f$, or equivalently $T$ as per Eq. (3.6). The spectator nucleon in the $(K^-,K)$ reaction on an $A=3$ target is not shown. The baryon-baryon-fusion vertex for $H$ formation is called $\Gamma$.

In Fig. 2, we display several higher-order processes which could contribute to $H$ production on a diproton pair. These processes lead to the $H$ via $\Lambda\Lambda$ or $\Sigma\Sigma$ fusion, and are expected to be much less important than the leading graph of Fig. 1. Following the method of Dover,[24] a very crude estimate can be obtained for the contribution of the graph in Fig. 2 involving an intermediate $\pi$ and di-$\Lambda$ production. The differential cross section ($K^+$ at 0°) for quasielastic $\Lambda\Lambda$ production, summed over all final states $f$, is given by[24]

$$\sum_f\left[\frac{d\sigma}{d\Omega_L}\right]_f^{0^\circ}\approx\frac{8\pi^2\xi}{p_\pi{}^2}\left\langle\frac{1}{r^2}\right\rangle\left[\alpha\frac{d\sigma}{d\Omega_L}\right]_{K^-p\to\pi^0\Lambda}^{0^\circ}\left[\alpha\frac{d\sigma}{d\Omega_L}\right]_{\pi^0p\to K^+\Lambda}^{0^\circ}\ ,$$

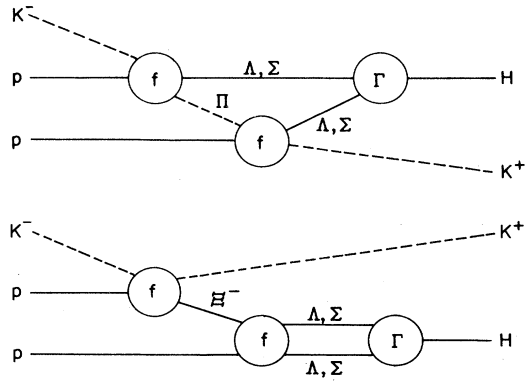


FIG. 2. Higher-order processes for $H$ production on a diproton in the $(K^-,K^+)$ reaction.

where $\xi \approx 0.019$ mb$^{-1}$ is a constant characteristic of the angular shape of the two-body angular distributions, $\langle 1/r^2 \rangle \approx 0.028$ mb$^{-1}$ is the mean inverse-square radial separation of the diproton, and $p_\pi$ is the laboratory pion momentum (assumed on-shell). For $k_L \approx 1.8$ GeV/$c$, we estimate that $\alpha d\sigma/d\Omega_L$ is about 0.2 mb/sr and 0.1 mb/sr for the $K^- p \to \pi^0 \Lambda$ and $\pi^0 p \to K^+ \Lambda$ reactions, respectively. This yields the estimate

$$\sum_f \left[ \frac{d\sigma}{d\Omega_L} \right]_f^{0^\circ} \approx 0.3 \ \mu\text{b/sr} \ .$$

Based on our calculations of $\Xi^- p \to H$ recombination reported in Sec. IV, we expect that the fusion probability for $H$ formation in $\Lambda\Lambda$ collisions does not exceed $10^{-3}$, so 0.3 nb/sr is an estimate of the $H$ cross section from the second-order process under consideration. This is much smaller than the value 0.3—0.5 $\mu$b/sr we obtain in Sec. IV for the lowest-order $H$-production process in Fig. 1. We do not expect much larger cross sections from other higher-order processes, and we neglect them in the subsequent discussion.

The evaluation of $M^{(3)}$ requires three important ingredients: $T$, $\psi_{\text{He}}$, and $\Gamma$. The first is the amplitude $T$ for the process $K^- p \to K^+ \Xi^-$. In general, we need an off-shell $T$-matrix element. Here, we always replace $T$ by an on-shell amplitude at energy

$$E = (m_K{}^2 + k_L{}^2)^{1/2} + (m_N{}^2 + p'^2)^{1/2} \ .$$

We restrict our attention to $K^+$ production in the forward direction ($\vec{k}' \| \vec{k}_L$), in order to keep the momentum transfer to the $^3$He target as small as possible. Thus, $T$ is a laboratory amplitude at $\theta_L = 0^\circ$ for the $K^+$. The data on the forward laboratory cross section $(d\sigma/d\Omega_L)^{0^\circ}_{K^- p \to K^+ \Xi^-}$ have been collected in Ref. 24 as a function of $K^-$ laboratory momentum $\vec{k}_L$. In this work, we use a simple parametrization of this data in the form

$$\left[ \frac{d\sigma}{d\Omega_L} \right]^{0^\circ}_{K^- p \to K^+ \Xi^-} \approx 66 \left[ 1 - \frac{k_{\text{thr}}{}^2}{k_L{}^2} \right]^{1/2} \exp\left[ - \left[ \frac{k_L - k_0}{\Delta k} \right]^2 \right] \quad (3.5)$$

in $\mu$b/sr, where $k_{\text{thr}} = 1.046$ GeV/$c$ is the laboratory threshold momentum, and $k_0 = 1.75$ GeV/$c$, $\Delta k = 0.6$ GeV/$c$. The available experimental data on the $K^- p \to K^+ \Xi^-$ forward cross section, together with their parametrization via Eq. (3.5), are shown in Fig. 3. One can also obtain more sophisticated parametrizations of

$$\left[ \frac{d\sigma}{d\Omega_L} \right]^{0^\circ}_{K^- p \to K^+ \Xi^-}$$

which treat the region near threshold more precisely. For instance, one can use the relation between $d\sigma/d\Omega_L$ and the invariant two-body amplitude $T$:

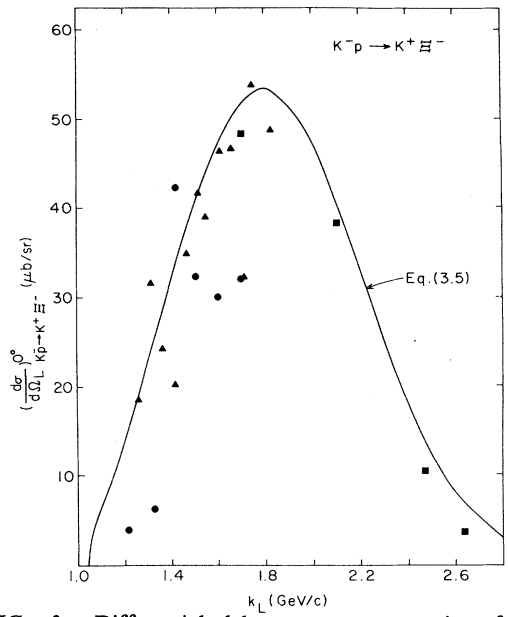


FIG. 3. Differential laboratory cross section for the $K^- p \to K^+ \Xi^-$ reaction in the forward direction as a function of $K^-$ laboratory momentum $k_L$. The experimental points are due to Dauber *et al.* (Ref. 25) (squares), Berge *et al.* (Ref. 26) (circles), and Burgun *et al.* (Ref. 27) (triangles). The data have been averaged over the small-angle region as discussed in Ref. 24. The solid curve is the parametrization of Eq. (3.5) used in the calculations reported here.

$$\left[ \frac{d\sigma}{d\Omega_L} \right]^{0^\circ}_{K^- p \to K^+ \Xi^-} = |f|^2 = \frac{(k_2')^2}{16\pi^2} |T|^2 / [\lambda(s_2, m_K{}^2, m_p{}^2) \lambda(s_2, m_K{}^2, m_\Xi{}^2)]^{1/2} \ , \quad (3.6)$$

where $s_2$ is the invariant mass-squared of the $K^- p$ system and $k_2'$ is the $K^+$ momentum in the two-body laboratory system. One could then parametrize $|T|^2$ directly rather than $|f|^2$. Since the kinematical factors relating these two quantities vary only rather slowly, this choice is not crucial. For producing the $H$ we are most interested in the region near $k_L \approx 1.8$ GeV/$c$, where $\Xi^-$ production is largest. Our results are thus not very sensitive to the threshold behavior of $d\sigma/d\Omega_L$. Note that the data displayed in Fig. 3 are rather scattered, even after angular smoothing, so there is perhaps a 30% normalization uncertainty in our results in any case.

Equation (3.5) gives $d\sigma/d\Omega_L$ in the two-body laboratory (2L) frame, where the proton is at rest. However, we need this cross section in the many-body laboratory (ML) frame, where the $^3$He nucleus is at rest, but where the struck proton in general has a finite momentum. For forward angles, the relation between these two cross sections is easily deduced from Eq. (3.6) to be

$$\left[ \frac{d\sigma}{d\Omega_L} \right]^{0^\circ}_{\text{ML}} = \left[ \frac{k'}{k_2'} \right]^2 \left[ \frac{d\sigma}{d\Omega_L} \right]^{0^\circ}_{\text{2L}} \ , \quad (3.7)$$

where $k'$ ($k_2'$) is the three-momentum of the $K^+$ in the many- (two-) body laboratory frame. In Eq. (3.7), we assume that all particles are on the mass shell.

The second ingredient in the evaluation of $M^{(3)}$ is the specification of the initial state. The $K^-$ wave function is taken to be a plane wave. For a light target like $^3$He, distortion effects are not expected to be large. The $^3$He nucleus is represented by an internal wave function $\psi_{\rm He}$ which depends only on the two relative coordinates, for which we use a simple Gaussian form. In coordinate space, the total $^3$He space wave function $\psi_{\rm He}$ then becomes

$$\psi_{\rm He}^{\vec{K}}(\vec{r}_1,\vec{r}_2,\vec{r}_3)=\sqrt{2E}\,e^{i\vec{K}\cdot(\vec{r}_1+\vec{r}_2+\vec{r}_3)}\psi_{\rm He}(\vec{\rho},\vec{\lambda})$$

with

$$\psi_{\rm He}(\vec{\rho},\vec{\lambda})=3^{-3/4}(\pi b^2)^{-3/2}e^{-(\rho^2+\lambda^2)/2b^2} \tag{3.8}$$

in terms of $\vec{\rho}=(\vec{r}_1-\vec{r}_2)/\sqrt{2}$ and $\vec{\lambda}=(\vec{r}_1+\vec{r}_2-2\vec{r}_3)/\sqrt{6}$, and $b=1.70$ fm, which allows one to reproduce the $^3$He rms radius[28] $\langle r^2\rangle^{1/2}=1.88$ fm.

In order to study the effect of short-range correlations in the $^3$He wave function on the cross sections for $H$ production, we have also used the following simple generalization of the wave function of Eq. (3.8):

$$\psi_{\rm He}(\vec{\rho},\lambda)=Ne^{-(\rho^2+\lambda^2)/2b'^2}\prod_{i<j}(1-ce^{-(\vec{r}_i-\vec{r}_j)^2/2a^2}) . \tag{3.9}$$

Here $N$ assures proper normalization. We have tried two distinct sets of parameters $\{b',c,a\}$ in Eq. (3.9). For the first set we took, in the spirit of Ref. 29, $a=0.315$ fm, $b'=1.688$ fm, and $c=1.0$. We refer to this choice as model I. These parameters reproduce the value $\langle r^2\rangle^{1/2}=1.88$ fm, and also the position of the first dip in the $^3$He charge form factor[28] $|F_{\rm ch}(q)|$ at $q^2=11.6$ fm$^{-2}$. The fit of model I to $|F_{\rm ch}(q)|$ is shown as a solid line in Fig. 4, along with the data of Ref. 28. Another choice of parameters which we call model II is due to Fearing[30]: $a=0.601$ fm, $b'=1.283$ fm, and $c=0.925$. Model II, shown as a dashed line in Fig. 4, does a better job of reproducing $|F_{\rm ch}|$ for larger values of $q$, but yields an rms radius $\langle r^2\rangle^{1/2}=1.37$ fm which is too small.

Another ingredient of our calculation is the description of the particles in the final state. The wave functions of the $K^+$, $H$, and the neutron are taken to be plane waves. The $H$ dibaryon is treated as a single particle of sharp

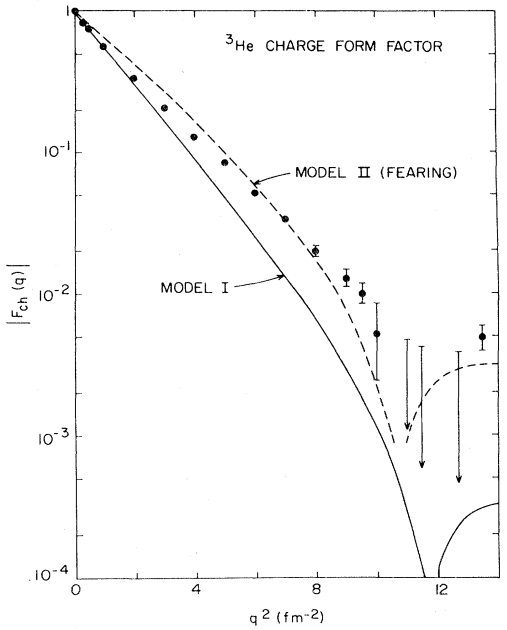


FIG. 4. Charge form factor $|F_{\rm ch}(q)|$ as a function of squared momentum transfer $q^2$ for $^3$He. The data are taken from McCarthy *et al.* (Ref. 29). The curves labeled model I and model II, defined in the text, correspond to two ways of parametrizing the short-range correlations in the $^3$He wave function, as per Eq. (3.9).

mass $m_H$ for purposes of imposing energy-momentum conservation, but its six-quark composite structure must be considered in deriving the form of the $\Xi^-p\to H$ fusion vertex $\Gamma$ in Eq. (3.3). The internal wave function of the $H$ is taken to be the six-particle version of Eq. (3.8), with the coordinates now referring to quark rather than nucleon positions. This microscopic description of the $H$ has the consequence that the internal structure of the $\Xi^-$ and the remaining proton in $^3$He (see Fig. 1) now is important. We assume that the internal wave function for these particles are also given by the Gaussian approximation of Eq. (3.8). The formation of the $H$ is thought of in terms of the fusion of two three-quark bags ($\Xi^-$ and $p$) into a six-quark bag. The amplitude $\Gamma(k_p,k_\Xi)$ for this fusion is approximated by the following wave-function overlap:

$$\Gamma(\vec{k}_p,\vec{k}_\Xi)=\frac{1}{(2\pi)^{18}}\int\frac{d^3k_1}{2E_1}\cdots\frac{d^3k_6}{2E_6}\psi_{H,\vec{k}_H}(\vec{k}_1\cdots\vec{k}_6)\psi_{p,\vec{k}_p}(\vec{k}_1,\vec{k}_2,\vec{k}_3)\psi_{\Xi^-,\vec{k}_\Xi}(\vec{k}_4,\vec{k}_5,\vec{k}_6) . \tag{3.10}$$

Using Gaussian wave functions, we find

$$\Gamma(\vec{k}_p,\vec{k}_\Xi)=(2\pi)^3(2E_H2E_p2E_\Xi)^{1/2}\delta^3(\vec{k}_H-\vec{k}_p-\vec{k}_\Xi)\Gamma(\vec{k}_p-\vec{k}_\Xi) , \tag{3.11}$$

where

$$\Gamma(\vec{k}_p-\vec{k}_\Xi)=\Gamma_0\left[\frac{2R_pR_H}{R_H^2+R_p^2}\right]^3\left[\frac{2R_\Xi R_H}{R_H^2+R_\Xi^2}\right]^3\left[\frac{8\pi R_H^2}{3}\right]^{3/4}e^{(-R_H^2)/12(\vec{k}_p-\vec{k}_\Xi)^2} \tag{3.12}$$

is the vertex appearing in Eq. (3.3). The factor $\Gamma_0$ is due to color-flavor-spin recoupling, as per Eq. (2.6). Note that Eq. (2.6) refers to the wave-function decomposition at short distances ("$r=0$"), where the six quarks of the $H$ are confined within one bag. For a pair of three-quark bags separated by a large distance $r$, the color confined com-

ponent $|8_c \otimes 8_c\rangle$, which dominates for $r=0$, must go to zero. In writing Eq. (3.12), we neglect dynamical distortions of the wave functions as the bags approach each other. We use static oscillator wave functions, and thus neglect a possible time dependence of $\Gamma$. These approximations seem adequate for these first rough estimates.

The salient feature of $\Gamma$ is its strong dependence on the relative momentum $\vec{k}_R = \vec{k}_p - \vec{k}_\Xi$ of the $\Xi^- p$ pair. Small values of $k_R$ are preferred for $H$ production in a baryon-baryon-fusion process. In the case of a nuclear target, the Fermi motion of the nucleons provides a region of phase space where $k_R$ is small.

In Eq. (3.12), $R_H$, $R_\Xi$, and $R_p$ are the oscillator parameters for the $H$, $\Xi^-$, and $p$, respectively. The value $R_p = 0.83$ fm chosen to reproduce the rms radius of the proton. In assigning values to $R_\Xi$ and $R_H$, we would like to take account of the fact that strange quarks have a larger mass parameter than nonstrange quarks, and therefore have a more localized space wave function. This would lead to small values for the rms radii of hadrons containing strange quarks, when compared to their nonstrange counterparts. No measured value for the rms radii of the $\Xi^-$ exists. Using the MIT bag model relation between the proton bag radius and that of the $\Xi^-$ we would arrive at $R_\Xi = 0.73$ fm. However, since $R_\Xi$ appears only in the geometric factor

$$\left[\frac{2R_\Xi R_H}{R_H^2 + R_\Xi^2}\right]^3 ,$$

taking $R_\Xi$ less than $R_p$ would only result in a reduction of a few percent in overall normalization. We will rather take $R_\Xi = R_p$ here. The choice of $R_H$ is more critical, since it appears in the Gaussian factor in Eq. (3.12). We use the relations of the rms radius $\langle r^2\rangle^{1/2}$ to the oscillator parameter $R_H(\langle r^2\rangle_H = \frac{5}{4}R_H^2)$ and to the bag radius $R_H$(bag) $[\langle r^2\rangle_H = 0.41 R_H^2(\text{bag})]$, and similarly for the proton: $\langle r^2\rangle_p = R_p^2$ and $\langle r^2\rangle_p = 0.53 R_p^2(\text{bag})$ to arrive at $R_H = R_p$ if $R_H(\text{bag}) \cong 2^{1/3} R_p(\text{bag})$. We thus adopt the value $R_H \cong 0.83$ fm, which then sets a scale for the range of $k_R$ values which offer a non-negligible contribution to the cross section for $H$ production, namely, $k_R \leq 0.6$ GeV/$c$.

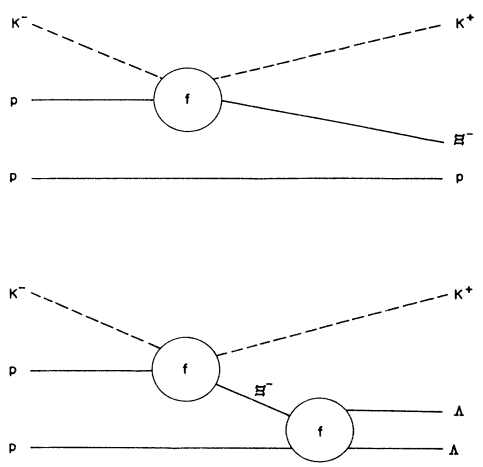


FIG. 5. Processes involving the $(K^-, K^+)$ reaction on a diproton pair which do not involve $H$ formation. These contribute to the "quasielastic background." If the $H$ is bound with respect to the $\Lambda\Lambda$ threshold, the $H$ signal can be distinguished from these backgrounds by a careful measurement of the $K^+$ momentum spectrum or the "missing-mass" spectrum involving the detection of the $K^+$ and neutron in coincidence in the $^3$He$(K^-, K^+ n)$ reaction.

In addition to $H$ production, $K^+$ mesons in the final state may also be associated with the "quasielastic" process (see Fig. 5)

$$K^- + {}^3\text{He} \rightarrow K^+ + n + p + \Xi^- . \tag{3.13}$$

The total cross section $\sigma_{\text{QE}}$ corresponding to this reaction may be written as

$$\sigma_{\text{QE}} = \frac{1}{(2\pi)^8} \int \frac{d^3k'}{2E_{k'}} \int \frac{d^3p_n}{2E_n} \int \frac{d^3k_p}{2E_p} \int \frac{d^3k_\Xi}{2E_\Xi} \delta^{(4)}(P - k' - p_n - k_p - k_\Xi) \, |M^{(4)}|^2 / 2\lambda^{1/2}(s, m_K^2, m_{\text{He}}^2) . \tag{3.14}$$

The differential momentum spectrum $d^2\sigma_{\text{QE}}/d\Omega_{K^+}dk'$ of the $K^+$ and the "missing-mass" spectrum $d^3\sigma_{\text{QE}}/d\Omega_{K^+}d\Omega_n ds$ for a $K^+$-neutron coincidence experiment may be obtained by appropriate differentiations of Eq. (3.14). The matrix element $M^{(4)}$ is given by

$$M^{(4)} = \left[\frac{2m_{\text{He}} 2E_p 2E_n}{2E_{p'}}\right]^{1/2} T(\vec{k}_L, \vec{p}\,'; \vec{k}', \vec{k}_\Xi) \psi_{\text{He}}(\vec{k}_\rho, \vec{k}_\lambda) , \tag{3.15}$$

where $\vec{p}\,'$, $\vec{k}_\rho$, and $\vec{k}_\lambda$ are defined in Eq. (3.4). In estimating the $K^+$ "background" from Eqs. (3.14) and (3.15), we neglect distortions of the $K^+$ spectrum due to final-state interactions, namely, $\Xi^- p$ elastic scattering or charge exchange and $\Xi^- p \rightarrow \Lambda\Lambda$ conversion.

Since the integrated quasielastic cross section for $K^+$ production is several orders of magnitude larger than that associated with $H$ production, it is not possible to find the $H$ by a measurement of $\sigma$ or $d\sigma/d\Omega_{K^+}$ alone. A careful study of the $K^+$ momentum spectrum or a $K^+$-neutron coincidence experiment is required. This is treated in the next section.

In addition to the $K^+$ quasielastic production, a background can also arise from $\pi^+$'s in the final state which are misidentified as $K^+$'s. Production of $\pi^+$'s is possible via a number of reactions; these are discussed in Sec. V.

## IV. RESULTS

In this section, we discuss our numerical results for the reaction $^3$He$(K^-, K^+)Hn$. Some preliminary results at a $K^-$ laboratory momentum of $k_L = 1.9$ GeV/$c$ were presented in Ref. 31. In this paper, we consider in detail

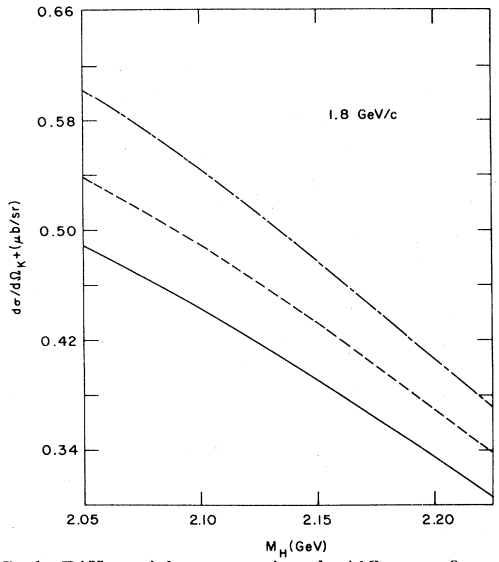


FIG. 6. Differential cross section $d\sigma/d\Omega_{K^+}$ at $\theta_{K^+}=0°$ for $H$ production in the $^3\mathrm{He}(K^-,K^+)nH$ reaction at laboratory momentum $k_L=1.8$ GeV/$c$, as a function of the mass $m_H$ of the $H$. The dashed curve corresponds to a calculation in which short-range correlations in the $^3$He wave function are neglected. The solid and dash-dot curves correspond to models I and II, respectively, for the $^3$He short-range correlations, as described in Sec. III.

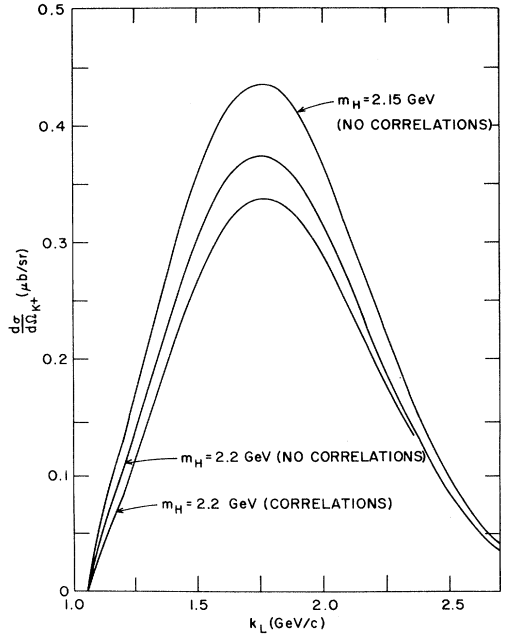


FIG. 7. Momentum dependence of the $^3\mathrm{He}(K^-,K^+)nH$ differential cross section at $\theta_{K^+}=0°$. The curves are labeled by the $H$ mass; $^3$He short-range correlations (model I) are included for the curve labeled "correlations."

the $k_L$ dependence of the cross sections, the influence of short-range correlations in the $^3$He wave function, and the problem of separating the $H$ signal from the continuum background of $\Xi^-p$ or $\Lambda\Lambda$ pairs.

First consider the single-differential cross section $d\sigma/d\Omega_{K^+}$, involving only $K^+$ direction. In Fig. 6, we display this cross section as a function of the rest mass of the $H$, for a fixed value of $k_L$. The curves show a monotonic decrease with $m_H$ as we approach the $\Lambda\Lambda$ threshold from below, reflecting the diminished phase space. The calculation would quickly lose its meaning above $m_H \approx 2m_\Lambda$, since we assume a stable bound-state Gaussian wave function for the $H$. The three curves in Fig. 6 demonstrate the effect of short-range correlations in the $^3$He wave function. The dashed curve assumes no correlations, i.e., $\psi_{\mathrm{He}}$ is just a product of Gaussians in the relative variables $\rho$ and $\lambda$ [see Eq. (3.7)]. The solid curve ( model I) incorporates a product of Gaussian correlation functions, as per Eq. (3.8), with parameters chosen to reproduce the rms radius of $^3$He, as well as the position of the first dip in the $^3$He charge form factor. The dot-dashed curve in Fig. 6, gives the result of using a correlation function due to Fearing[30] (model II). We see from Fig. 6 that the two models for short-range correlations bracket the result which obtains in the limit of no correlations. The uncertainty in our results due to correlations is seen to be only $\pm 10\%$. One might naively expect that short-range correlations in $^3$He must substantially lower the $H$-production cross section. This is not true, since the $K^-p\to K^+\Xi^-$ process involves *high momentum transfer* ($\approx$400 MeV/$c$), and hence a small relative separation (in momentum space) for the $\Xi^-p$ pair (which is required for $H$ formation) does not necessarily imply a small separation for the initial $pp$ pair. For high $q$ processes, short-range correlations can even produce some increase in the cross section (the dot-dashed curve in Fig. 6), since they can supply needed higher momentum components for the second proton which fuses with the generally high momentum $\Xi^-$.

The momentum dependence of the $^3\mathrm{He}(K^-,K^+)nH$ cross section $d\sigma/d\Omega_{K^+}$ is shown in Fig. 7. The results mirror the strong momentum dependence of the two-body cross section for $K^-p\to K^+\Xi^-$, shown in Fig. 3, with a slight broadening due to the Fermi motion of the protons in $^3$He. This is true because the Fermi momentum is small compared to $k_L$, and the two-body momentum transfer decreases only rather slowly above $k_L \approx 1.4$ GeV/$c$. Figure 7 also demonstrates that the effect of correlations is rather similar for all values of $k_L$. If one compares the values of $d\sigma/d\Omega_{K^+}$ for $H$ production with the total 0° cross section for $\Xi^-p$ continuum pair production [$\approx 2(d\sigma/d\Omega)_{K^-p\to K^+\Xi^-}$, neglecting any absorptive effects], one gets a rough estimate for the probability $P_{\Xi^-p\to H}$ of $H$ production in $\Xi^-p$ collisions, namely,

$$P_{\Xi^-p\to H} \approx 4\times 10^{-3} \tag{4.1}$$

for $m_H \approx 2200$ MeV. This small probability reflects the fact that $H$ production occurs only when the $\Xi^-p$ relative momentum is small, and this condition is satisfied only in a very restricted region of the phase space supplied by the $^3$He wave function.

We now turn to a discussion of the $K^+$ momentum spectrum. In Fig. 8, we display the $K^+$ double-

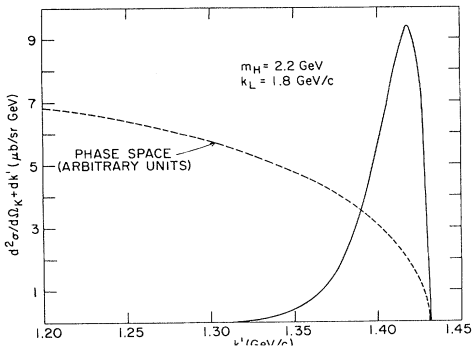


FIG. 8. The $K^+$ momentum spectrum in the reaction $^3\text{He}(K^-,K^+)nH$ for $\theta_{K^+}=0°$; $k'$ is the laboratory momentum of the $K^+$. The solid curve represents the exact calculation, including short-range correlations (model I). The dashed curve shows the $K^+$ momentum distribution which results from three-body phase space alone, without effects of the $^3$He wave function or the $\Xi^-p\to H$ fusion vertex.

differential cross section $d^2\sigma/d\Omega_{K^+}dk'$ for the $^3\text{He}(K^-,K^+)nH$ reaction at 1.8 GeV/$c$ and $\theta_{K^+}=0°$, as a function of the magnitude $k'$ of the $K^+$ laboratory momentum. The $K^+$ momentum spectrum is seen to be sharply peaked very near to the maximum momentum allowed by the relativistic phase space. If we had used a pure three-body phase-space factor to estimate the shape of the $K^+$ spectrum, we would have obtained the much more spread out momentum distribution indicated by the dashed line in Fig. 8. The sharp peaking in $k'$ is due to the dynamics of the $(K^-,K^+)$ reaction mechanism (see Fig. 3). On the one hand, the quark-fusion vertex $\Gamma$ requires *small* relative $\Xi^-p$ momentum $\vec{k}_\Xi-\vec{k}_p$; the $^3$He wave function, on the other hand, provides only relatively small momenta (of order 250 MeV/$c$ or less) $\vec{k}_p$ for the proton to match to the typically rather large (of order 400 MeV/$c$) value of $\vec{k}_\Xi$. The possibility of achieving small values of $\vec{k}_\Xi-\vec{k}_p$ is enhanced if the overall momentum transfer $q=k_L-k'$ and thereby $\vec{k}_\Xi$ is made as small as possible. Hence the cross section must peak near the maximum allowable value of $k'$. In the present case, the momentum transfer $q\geq 366$ MeV/$c$ (at $k_L=1.8$ GeV/$c$) always remains larger than the Fermi momentum $k_F$, so $\vec{k}_\Xi$ and $\vec{k}_p$ are generally mismatched. The optimum $q$ would presumably be of order $k_F$, but this value is not allowed by energy-momentum conservation.

The focusing of $k'$ near the maximum value allowed by phase space is a general feature for all values of $k_L$, as seen in Fig. 9. As $k_L$ decreases, the minimum value of $q$ increases slightly, but the shapes of the various $K^+$ spectra remain very much the same. If we integrate over $k'$, we of course recover the lower solid curve in Fig. 7, which peaks near $k_L\approx 1.8$ GeV/$c$.

In assessing the significance of the narrow peak in the $K^+$ spectrum for $H$ production, one must ask how it compares with the momentum spectrum of "background" $K^+$'s recoiling against continuum $\Xi^-p$ pairs. For the background, we have a four-particle phase space; here one proton and the neutron are spectators. The calculation of the background spectrum is described in Sec. III: it is generated by the mechanism shown in Fig. 5. It is clear that the maximum value $k'_{\max}$ of $k'$ in the background spectrum must lie below that for the $H$ production if $m_H<m_p+m_\Xi$. Since the full width at half maximum of the peaks in Fig. 8 is only about $\Delta k'\approx 30$ MeV/$c$ independent of $k_L$ (in the range 1.4—2.2 GeV/$c$), it should be possible in principle to separate the $H$ production from the $\Xi^-p$ background by a careful measurement of the $K^+$ momentum spectrum (the values of $k'_{\max}$ for $\Xi^-p$ and $H$ production differ by about 75 MeV/$c$ for $m_H=2.2$ Gev/$c$).

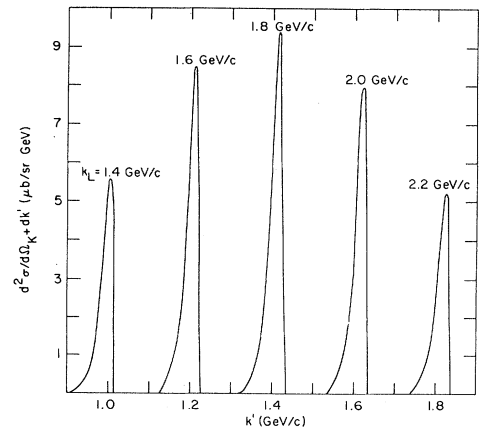


FIG. 9. The differential $^3\text{He}(K^-,K^+)nH$ cross section $d^2\sigma/d\Omega_{K^+}dk'$ as a function of the $K^+$ momentum $k'$, for several choices of the incident $K^-$ momentum $k_L$. The $K^+$ angle (0°) and the $H$ mass (2.2 GeV) are fixed. Short-range correlations in $^3$He are included (model I).

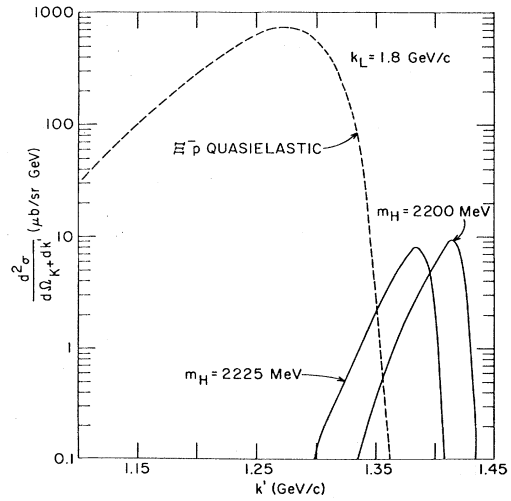


FIG. 10. Cross sections $d^2\sigma/d\Omega_{K^+}dk'$ for the $(K^-,K^+)$ reaction on $^3$He at $k_L=1.8$ GeV/$c$ and $\theta_{K^+}=0°$. The solid curves correspond to $H$ production for two different $H$ masses (correlations included in model I). The dashed curve corresponds to the continuum background arising from the reaction $^3\text{He}(K^-,K^+)n\Xi^-p$.

In Fig. 10 we plot the $K^+$ spectrum corresponding to both $H$ and $\Xi^- p$ continuum production. The continuum spectrum peaks at $q \approx 525$ MeV/$c$, very close to the momentum transfer for the two-body $K^- p \to K^+ \Xi^-$ reaction on a proton at rest. Its width is related to the momentum content of the $^3$He wave function. Although the continuum cross section is roughly 100 times larger at peak than that for $H$ production, Fig. 10 suggests that the two processes can be distinguished if one can measure the $K^+$ momentum to 2% or better ($\Delta k'/k' \approx 30/1400$). However, if the $H$ lies too close to threshold, it will be difficult to see in view of the intrinsically much larger size of the background. Note that in Fig. 10, we have considered only the $\Xi^- p$ continuum. Due to higher-order processes (see Fig. 2), for instance, $\Xi^- p \to \Lambda\Lambda$ conversion in the final state, there will be some seepage of cross section into the $\Lambda\Lambda$ continuum channel. Since the $\Lambda\Lambda$ threshold lies 30 MeV below that for $\Xi^- p$, and the corresponding value of $k'_{\max} \approx 1.393$ GeV/$c$ is somewhat larger, the combined $\Xi^- p + \Lambda\Lambda$ background spectrum will be slightly distorted from that shown in Fig. 10, and will extend to somewhat higher momentum. Estimates of the conversion cross section $(v\sigma)_{\Xi^- p \to \Lambda\Lambda}$ have been made by Macek *et al.*,[28] based on the one-boson-exchange picture of the Nijmegen group[21] (model F); for a spin and isospin singlet $\Xi^- p$ pair, they obtain a small value $(v\sigma)^{S=I=0}_{\Xi p \to \Lambda\Lambda} \approx 10$ mb by solving coupled equations. A somewhat larger estimate of 60 mb was obtained in perturbation theory by Dover and Gal[29] using model D of Ref. 21; this is probably an upper bound. In any case, it is not likely that $\Xi^- p \to \Lambda\Lambda$ conversion, for which the cross section is of normal size, will produce any qualitative modifications of the continuum spectrum, although we have not made detailed estimates.

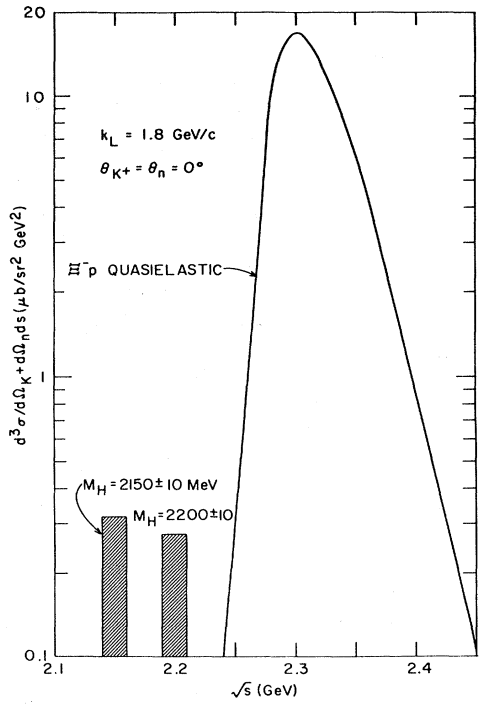


FIG. 12. The "missing-mass" spectrum for the $^3$He$(K^-,K^+n)H$ or $^3$He$(K^-,K^+n)\Xi^- p$ reactions at 1.8 GeV/$c$. The $K^+$ and neutron are detected in coincidence at 0°. The invariant mass of the $\Xi^- p$ system is $\sqrt{s}$. The solid curve is the $\Xi^- p$ continuum cross section, while the cross-hatched bars correspond to production of the bound $H$ dibaryon (for two different masses of the $H$). An experimental mass resolution of ±10 MeV is arbitrarily assumed in the region of the $H$.

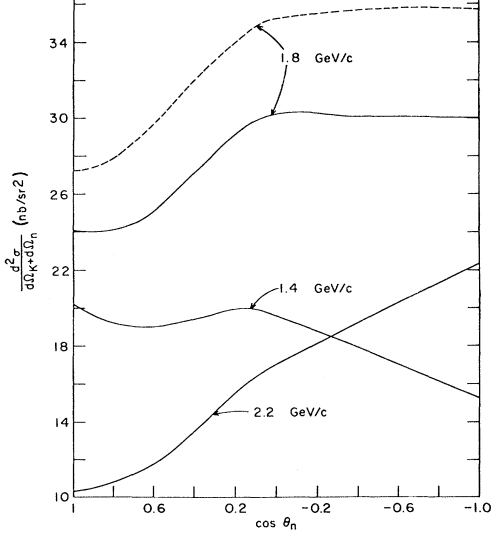


FIG. 11. Double-differential cross sections $d^2\sigma/d\Omega_{K^+} d\Omega_n$ for the $^3$He$(K^-,K^+n)H$ reaction, for $\theta_{K^+} = 0°$, as a function of the cosine of the neutron laboratory angle. The curves are labeled by the $K^-$ laboratory momentum. The solid curves refers to $m_H = 2.2$ GeV, while the dashed curve for $k_L = 1.8$ GeV/$c$ corresponds to $m_H = 2.15$ GeV.

Although in principle one could see a distinct signature of the $H$ in the $K^+$ momentum spectrum, in practice there may be sources of background in the vicinity of $k' \approx 1.4$ GeV/$c$ where the $H$ signal is localized (for $k_L \approx 1.8$ GeV/$c$). We consider a possible background from misidentified $\pi^+$'s in Sec. V. The detection of the final-state neutron in coincidence with the $K^+$ could serve to reduce certain backgrounds. This may outweigh the loss in counting rate incurred by requiring a coincidence. The laboratory angular distributions of the neutrons in the $^3$He$(K^-,K^+n)H$ reaction at various $K^-$ momenta and $\theta_{K^+} = 0°$ are shown in Fig. 11. The neutrons switch from being forward peaked at low $k_L$ to backward peaking at higher momenta. The solid and dashed curves for 1.8 GeV/$c$ refer to $m_H = 2.2$ and 2.15 GeV, respectively; the angular distribution of the neutron is seen to vary only slightly in shape for these two cases. The change from forward to backward peaking is a simple kinematical effect: for momenta close to the $H$-production threshold, all the reaction products will be produced in a forward cone in the laboratory, while for higher momenta the lighter neutron prefers the backward direction in the laboratory while the heavier $H$ goes forward.

The virtue of measuring the $K^+$ and neutron in coincidence in the $^3$He$(K^-,K^+n)H$ reaction is that the only "missing mass" is the $H$ itself. In a plot of the cross sec-

tion $d^3\sigma/d\Omega_{K^+}d\Omega_n ds$ for fixed $K^+$ and neutron angles, as a function of the invariant mass $\sqrt{s}$ of the recoiling $\Xi^- p$ pair, one should see a sharp peak at the $H$ mass, if the $H$ is a bound state. Such a plot is shown in Fig. 12. The cross-hatched bars correspond to $H$ production, assuming two different values for $m_H$. An experimental mass resolution of $\pm 10$ MeV was arbitrarily assumed (the intrinsic width of the $H$ peak is essentially zero). The background due to the formation of $\Xi^- p$ continuum pairs is shown as a solid curve in Fig. 12. If the $H$ is bound, it should be clearly separable from the continuum background in such a "missing mass" plot. However, if the $H$ lies above threshold, it will be very difficult to disentangle from the much larger background cross section.

All of our results correspond to forward $K^+$ production, which is the optimal case. Since the momentum transfer in the $(K^-,K^+)$ reaction is quite large even for $\theta_{K^+}=0°$, the cross section for $H$ production is expected to drop off smoothly as $\theta_{K^+}$ increases. Our calculations have also assumed the plane-wave approximation for the $K^-$, $K^+$, $H$, and $n$ wave functions. There is some absorption of the $K^-$ in the initial state, which will diminish the $H$-production cross section somewhat. However, since the $^3$He target is so light, this is not expected to lead to a dramatic effect. The $K^+$ in the final state has a rather small cross section for interaction with the neutron, and the $H$ and neutron are anticorrelated in angle for larger $k_L$ so their interaction will not be significant. Thus the plane-wave approximation is expected to be adequate for the present estimates.

## V. BACKGROUNDS FROM $\pi^+$ PRODUCTION

As seen in Fig. 9, $H$ production in the $(K^-,K^+)$ reaction on $^3$He is characterized by a sharp peak in the $K^+$ momentum spectrum, corresponding to a momentum transfer of about 400 MeV/$c$. For example, at $k_L \approx 1.8$ GeV/$c$, the maximum of the $H$-production cross section, the $K^+$ spectrum is peaked at $k' \approx 1.42$ GeV/$c$, for a choice $m_H = 2200$ MeV. Since the $K^+$ at this momentum is relativistic ($\beta = v/c = 0.9445$), a $\pi^+$ at the same momentum ($\beta = 0.9952$) may occasionally be misidentified as a $K^+$, providing another background for $H$ production. Thus we have considered reactions of the type

$$K^- + {}^3\mathrm{He} \rightarrow \pi^+ + X \tag{5.1}$$

as potential backgrounds. In Table II, we give the two-body total cross sections[32] for $\pi^+$ production in the $K^- p$ reaction at $k_L = 1.8$ GeV/$c$, together with the maximum attainable value $(k')_{\max}$ for the $\pi^+$ momentum. In Table III, we provide the corresponding values of $(k')_{\max}$ for $K^+$ production channels

$$K^- + {}^3\mathrm{He} \rightarrow K^+ + X \ . \tag{5.2}$$

According to Table III, we have $(k')^{\Lambda\Lambda n}_{\max} = 1.393$ GeV/$c$ for the $K^- + {}^3\mathrm{He} \rightarrow K^+ + \Lambda\Lambda n$ process. If the $H$ is unbound with respect to the $\Lambda\Lambda$ threshold, we have $(k')^{Hn}_{\max} < (k')^{\Lambda\Lambda n}_{\max}$; in this regime the $H$ will merge into the $\Lambda\Lambda$ quasielastic background, and will be difficult if not impossible to detect. If we assume that the $H$ is stable, then $(k')^{Hn}_{\max} > (k')^{\Lambda\Lambda n}_{\max}$. In this regime, reactions of type (5.1) with $(k')_{\max} < (k')^{\Lambda\Lambda n}_{\max}$ are of no consequence, since they produce only $\pi^+$'s of lower momentum than the $K^+$'s associated with $H$ production. For this reason, open channels of the type $K^- p \rightarrow \pi^+ \Lambda(n\pi)$ or $\pi^+ \Sigma(n'\pi)$ with $n \geq 3$ and $n' \geq 2$ have been omitted from Table II. These

TABLE II. Values of $(k')_{\max}$ and two-body total cross section[32] for $K^- + {}^3\mathrm{He} \rightarrow \pi^+ + X$ reactions.

| Missing mass $X$ | $(k')_{\max}$ (GeV/$c$) | $\sigma_{\mathrm{tot}}^{K^- p \rightarrow \pi^+ X'}$ (mb) |
|---|---|---|
| $\Sigma^- pn$ | 1.586 | 0.23 |
| $\Lambda\pi^- pn$ | 1.523 | 1.7 |
| $(\pi^-\Sigma^0 + \pi^0\Sigma^-)pn$ | 1.437 | 1.5 |
| $\Lambda\pi^-\pi^0 pn$ | 1.371 | 2.3 |
| $K^- npn$ | 1.322 | 2.8 |
| $(n\bar{K}^0 + pK^-)\pi^- pn$ | (1.188, 1.157) | 1.4 |
| $\Sigma^-\pi^- pp$ | 1.43 | $0.6(K^- n)$ |

TABLE III. Values of $(k')_{\max}$ for $K^- + {}^3\mathrm{He} \rightarrow K^+ + X$ reactions.

| Missing mass $X$ | $(k')_{\max}$ (GeV/$c$) |
|---|---|
| $Hn$ | 1.426 ($m_H = 2200$ MeV) |
| $\Lambda\Lambda n$ | 1.393 |
| $\Xi^- pn$ | 1.358 |
| $\Xi^0\pi^- pn$ | 1.185 |
| $\Xi^-\pi^0 pn$ | 1.151 |

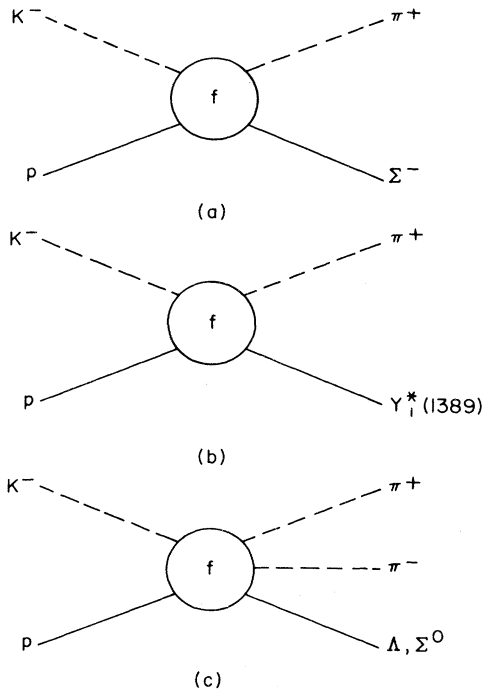


FIG. 13. Processes which generate a $\pi^+$ background.

channels tend to have small cross sections ($\sigma_{\text{tot}} \leq 0.2$ mb). An inspection of Table II then discloses that only the reactions

$$K^- p \to \pi^+ \Sigma^- , \tag{5.3a}$$

$$K^- p \to \pi^+ \pi^- \Lambda , \tag{5.3b}$$

$$K^- p \to \pi^+ (\pi^0 \Sigma^- + \pi^- \Sigma^0) , \tag{5.3c}$$

$$K^- n \to \pi^+ \pi^- \Sigma^- , \tag{5.3d}$$

can produce a $\pi^+$ background in the $K^+$ momentum region corresponding to $H$ production. The production of $\pi\pi\Sigma$ final states [reactions (5.3c) and (5.3d)] is mostly nonresonant in the region of interest and is similar to that of the $\pi\pi\Lambda$ nonresonant contribution. The $\pi\pi\Sigma$ channels only play a role when the $H$ lies close to the $\Lambda\Lambda$ threshold ($2200 < m_H < 2230$ MeV); we have omitted them here. The dominant processes of Eq. (5.3) are illustrated in Fig. 13.

Consider first reaction (5.3a), which provides the most important source of background for larger values of $k'$. Partial wave amplitudes for momenta up to $k_L \approx 1.4$ GeV/$c$ have been obtained by Gopal *et al.*[33] In the region from 1.2 to 1.4 GeV/$c$, the forward laboratory cross section is approximately described by the simple form

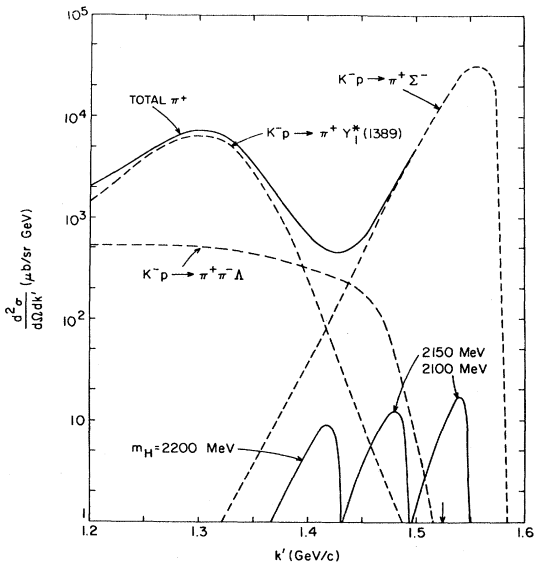


FIG. 14. Momentum spectra $d^2\sigma/d\Omega\, dk'$ for $\pi^+$ and $K^+$ production in the $K^- + {}^3\text{He}$ reaction at $k_L = 1.8$ GeV/$c$. The dashed curves correspond to quasielastic $\pi^+$ production in reactions (5.3a) and (5.3b). The curve labeled "$K^- p \to \pi^+ \pi^- \Lambda$" corresponds to nonresonant production in (5.3b) and that labeled "$K^- p \to \pi^+ Y_1^*(1389)$" corresponds to resonance formation. The summed $\pi^+$ cross section is labeled "total $\pi^+$." For comparison, the $K^+$ momentum spectrum for $H$ production is also shown for three values of the $H$ mass.

$$\left[\frac{d\sigma}{d\Omega_L}\right]^{0^\circ}_{K^- p \to \pi^+ \Sigma^-} \approx 0.244 + 1.062/k_L \tag{5.4}$$

in mb/sr, where $k_L$ is given in GeV/$c$. At 1.8 and 1.95 GeV/$c$, Dauber *et al.*[34] have determined Legendre coefficients for the $K^- p \to \pi^+ \Sigma^-$ angular distribution. Using their values,[34] we find

$$\left[\frac{d\sigma}{d\Omega_L}\right]^{0^\circ}_{K^- p \to \pi^+ \Sigma^-} \approx \begin{cases} 1.39 \text{ mb/sr at } 1.8 \text{ GeV}/c , \\ 0.58 \text{ mb/sr at } 1.95 \text{ GeV}/c , \end{cases} \tag{5.5}$$

indicating a rapid energy dependence of the cross section near the region $k_L \approx 1.8$ GeV of interest to us. This energy variation is interpreted in terms of resonance formation by Dauber *et al.*[34] Rather than assuming some resonance form for $d\sigma/d\Omega_L$, we simply use the smooth form (5.4), which produces about 0.8 mb/sr around $k_L \approx 1.8$–$1.9$ GeV/$c$, not far from the average of the two values in Eq. (5.5). Using Eqs. (5.4) and (3.6), we can construct the invariant two-body amplitude $T$. This is then inserted in Eqs. (3.14) and (3.15) to evaluate the quasielastic cross section for $\pi^+$ production.

The $\pi^+$ momentum spectrum arising from the $K^- p \to \pi^+ \Sigma^-$ reaction is shown as a dashed line in Fig. 14. At $k_L = 1.8$ GeV/$c$, the forward *two-body* momentum transfer for this process is $q(0^\circ) \approx 0.22$ GeV/$c$, so we expect the peak in the $\pi^+$ spectrum to occur near $k' \approx k_L - q(0^\circ) \approx 1.58$ GeV/$c$. Since this value of $k'$ is very close to the kinematical limit $(k')_{\max} = 1.586$ GeV/$c$ determined by *many-body* kinematics, the peak in fact occurs at slightly lower momentum $k' \approx 1.56$ GeV/$c$ in Fig. 14.

In Fig. 14, we also show the cross sections $d^2\sigma/d\Omega dk'$ for $H$ production, assuming various mass values for the $H$. As the $H$ mass decreases, the $H$ peak moves to higher values of $k'$ according to

$$(k')_{\text{peak},H} \approx 1.42 + 1.2(2.2 - m_H) , \tag{5.6}$$

where all quantities are in GeV/$c$. If $m_H \leq 2.05$ GeV, an unlikely possibility, the value of $(k')_{\text{peak},H}$ becomes larger than $(k')_{\max}$ for any possible $\pi^+$ or $K^+$ production process, and no background can mask the $H$ peak. For $m_H \approx 2.08$ GeV, the $\pi^+$ peak from $K^- p \to \pi^+ \Sigma^-$ and the $H$ peak coincide; in this mass region, one would be required to discriminate $\pi^+$'s from $K^+$'s to about 1 part in $10^3$.

A more likely case corresponds to an $H$ which lies not far from the $\Lambda\Lambda$ threshold ($2.2 \leq m_H \leq 2.23$ GeV). In this region, the most important $\pi^+$ background arises from the $K^- p \to \pi^+ \pi^- \Lambda$ reaction of Eq. (5.3b). This reaction has been studied in detail in the region $1.2 \leq k_L \leq 1.7$ GeV/$c$ by Huwe.[35] For $k_L \leq 1.6$ GeV/$c$, the quasi-two-body processes $K^- p \to \pi^- + Y_1^{*+}(1389)$ and $K^- p \to \pi^+ + Y_1^{*-}(1389)$ dominate the cross section, while for $k_L > 1.6$ GeV/$c$, the nonresonant $K^- p \to \pi^+ \pi^- \Lambda$ contribution increases rapidly.

Consider first the $K^- p \to \pi^+ + Y_1^{*-}(1389)$ reaction. Using the Legendre expansions given by Huwe,[35] we obtain for a forward $\pi^+$:

$$\left[\frac{d\sigma}{d\Omega_L}\right]^{0^\circ}_{K^-p\Rightarrow\pi^+Y_1^{*-}(1389)} \approx \begin{cases} 0.5\pm0.14 \text{ mb/sr for } 1.15<k_L<1.3 \text{ GeV}/c\ , \\ 0.45\pm0.27 \text{ mb/sr for } 1.3<k_L<1.45 \text{ GeV}/c\ , \\ 0.31\pm0.17 \text{ mb/sr for } 1.45<k_L<1.6 \text{ GeV}/c\ , \\ 0.41\pm0.05 \text{ mb/sr for } 1.6<k_L<1.75 \text{ GeV}/c\ . \end{cases} \tag{5.7}$$

A least-squares fit to these data with the form

$$\left[\frac{d\sigma}{d\Omega_L}\right]^{0^\circ}_{K^-p\to\pi^+Y_1^{*-}(1389)} = \alpha(1+\beta/k_L) \tag{5.8}$$

yields $\alpha=0.206$ mb/sr, $\beta=1.6$ GeV/$c$, with $k_L$ in GeV/$c$. For $K^-p\to\pi^-Y_1^{*+}(1389)$, we can also obtain a forward $\pi^+$ from $Y_1^{*+}$ decay; we expect a contribution comparable to Eq. (5.8), which we omit here.

The approximation (5.8) has been used to obtain the $\pi^+$ spectrum in the reaction $K^- + {}^3\text{He}\to\pi^+Y_1^{*-}(1389)pn$ at $k_L=1.8$ GeV/$c$. The results are shown as a dashed line in Fig. 14. Note that if we use a sharp mass of 1389 MeV for the $Y_1^*$, we obtain $(k')_{\max}=1.372$ GeV/$c$, which lies in the region below the $H$ peaks in Fig. 14. To obtain the tail of the $\pi^+$ spectrum extending beyond $k'\approx1.4$ GeV/$c$, we take account of the width $\Gamma\approx40$ MeV of the $Y_1^{*-}(1389)$. To do this, we perform calculations for a number of different mass values $E$ for the $Y_1^{*-}$, and add these contributions with the appropriate Breit-Wigner weight.

To obtain the contribution of the nonresonant reaction $K^-p\to\pi^+\pi^-\Lambda$ to the $\pi^+$ spectrum, we have simply used a constant value for $|T|^2$, adjusted to reproduce the average total cross section given by Huwe.[35] This gives the dashed curve labeled $K^-p\to\pi^+\pi^-\Lambda$ in Fig. 14. Due to the broader range of values for the effective mass of the recoiling $\pi^-\Lambda$ system in a nonresonant process, the resulting $\pi^+$ spectrum is more spread out in $k'$ than that for $Y^{*-}$ production.

In Fig. 14, we plot as a solid line the summed contributions of the $K^-p\to\pi^+\Sigma^-$, $\pi^+Y_1^{*-}(1389)$, and $\pi^+\pi^-\Lambda$ (nonresonant) processes to the $\pi^+$ spectrum. The sum displays a minimum around $k'\approx1.42$–$1.43$ GeV/$c$, corresponding to the $K^+$ peak for $H$ production with $m_H=2.2$ GeV. The combined $\pi^+$ spectrum is roughly 50 times as large as the $H$ signal in this domain, so even here a very good $\pi^+/K^+$ discrimination is required.

The cross sections for $\pi^+$-neutron or $K^+$-neutron coincidences are shown in Fig. 15. If $m_H<2.2$ GeV, only the $K^-p\to\pi^+\Sigma^-$ channel offers a serious $\pi^+$ background. For $m_H>2.2$ GeV, the $K^-p\to\pi^+\pi^-\Lambda$ reaction rapidly increases in importance as a source of background. Measuring the neutron in coincidence does not free one of the problem of background; good $\pi^+/K^+$ discrimination is still required, as in the study of the $K^+$ momentum spectrum. As a means of suppressing $\pi^+$ background, a trigger could be considered which vetoes events in which a $\Sigma^-$ is produced.

The conclusion of this section is that a study of $H$ production in the $K^- + {}^3\text{He}\to K^+ + H + n$ reaction is feasible, if careful consideration is given to the suppression of backgrounds due to misidentified $\pi^+$'s. Discrimination of $\pi^+$'s from $K^+$'s at the level of 1:100 is indicated in order to achieve an observable $H$ signal.

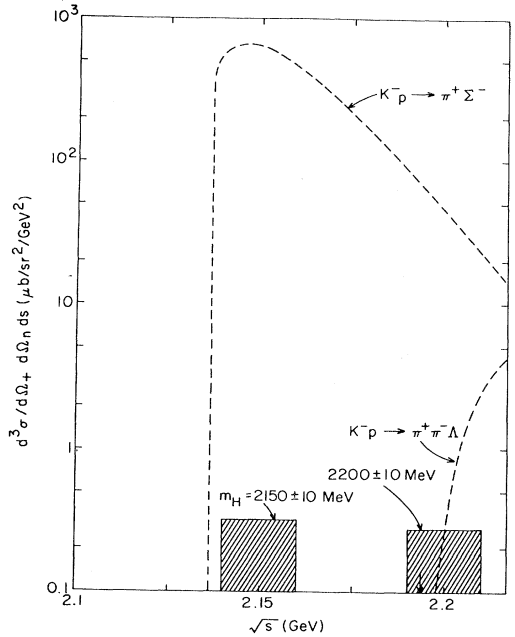


FIG. 15. Missing-mass spectra for $\pi^+$ and $K^+$ production in the $K^- + {}^3\text{He}\to(\pi^+ \text{ or } K^+) + X$ reactions at $k_L=1.8$ GeV/$c$. The dashed curves correspond to quasielastic $\pi^+$ production in coincidence with a recoiling spectator neutron. The cross-hatched boxes represent $H$ production, for two values of the $H$ mass.

## VI. SUMMARY

We have estimated cross sections for the production of the doubly strange $H$ dibaryon ($J^\pi=0^+$, $I=0$) in the reaction ${}^3\text{He}(K^-,K^+)nH$. It is argued that the $\Delta S=2$ strangeness-exchange reaction offers an optimum channel for manufacturing the $H$, preferable to reactions in which no strangeness is present in the initial state. Further, the prototype reaction $K^- + (pp)\to K^+ + (\Xi^-p)$ on a bound diproton, followed by $\Xi^-p\to H$ fusion, offers the most favorable combination of spin and isospin quantum numbers.

The $H$ may be seen either as a sharp peak in the $K^+$ momentum spectrum, or as a peak in a "missing-mass" plot in which the $K^+$ and neutron are detected in coincidence. In both cases, the $H$ signal may be separated from the background spectrum due to $\Xi^-p$ or $\Lambda\Lambda$ continuum states. The suppression of backgrounds due to $\pi^+$ production in a variety of reactions requires good $\pi^+/K^+$ discrimination. If the $K^+$-neutron coincidence mode is

selected, $^3$He is the best target, since the "missing mass" is the $H$ alone. If only the $K^+$ momentum spectrum is measured, a $^4$He target may serve as well as $^3$He.

The $K^+$-neutron coincidence cross sections for $H$ production are found to be rather small, some 25—30 nb/sr$^2$ for $\theta_{K^+}=0°$ and $k_L=1.8$ GeV/$c$ and a neutron in the forward hemisphere. These cross sections follow the $K^-$ momentum dependence of the elementary $K^-p\to K^+\Xi^-$ process, which has a maximum around $k_L\approx 1.8$ GeV/$c$. An intense $K^-$ beam in the momentum range of 1.6—2 GeV/$c$ is thus required. Such an experiment may be feasible with currently available $K^-$ beam intensities, but would be much easier at a future "kaon factory." The search for the $H$ dibaryon deserves very high priority. The $H$ plays a unique role in multiquark physics, since it is the *only* dibaryon which could lie well below all relevant strong-decay thresholds.

## ACKNOWLEDGMENTS

The authors would like to thank P. Barnes, R. H. Dalitz, and E. V. Hungerford for useful discussions. This work was supported by the U.S. Department of Energy under Contract No. DE-AC02-76CH00016.

[1]A. Chodos *et al.*, Phys. Rev. D 9, 3471 (1974); T. DeGrand *et al.*, *ibid.* 12, 2060 (1975).
[2]G. C. Rossi and G. Veneziano, Phys. Rep. 63, 149 (1980); T. Kamae, Nucl. Phys. A374, 25c (1982).
[3]B. R. Martin, in *Proceedings of the Topical Conference on Baryon Resonances, Oxford, England, July, 1976,* edited by R. T. Ross and D. H. Saxon (Rutherford Laboratory, Oxford, 1976), p. 409.
[4]D. Bugg, Nucl. Phys. A374, 95c (1982).
[5]T. H. Tan, Phys. Rev. Lett. 23, 395 (1969); O. Braun *et al.*, Nucl. Phys. B124, 45 (1977).
[6]B. J. VerWest, Phys. Lett. 83B, 161 (1979); B. Blankleider and I. R. Afnan, Phys. Rev. C 22, 1638 (1980).
[7]R. H. Dalitz and A. Deloff, Czech. J. Phys. B 32, 1021 (1982).
[8]R. L. Jaffe, Phys. Rev. Lett. 38, 195 (1977); 38, 1617(E) (1977).
[9]A. T. M. Aerts, University of Nijmegen thesis, 1979 (unpublished).
[10]P. J. G. Mulders, University of Nijmegen thesis, 1980 (unpublished).
[11]A. T. M. Aerts, P. J. G. Mulders, and J. J. de Swart, Phys. Rev. D 17, 260 (1978).
[12]R. L. Jaffe, Phys. Rev. D 15, 267 (1977); 15, 281 (1977).
[13]K. F. Liu and C. W. Wong, Phys. Lett. 113B, 1 (1982).
[14]P. J. G. Mulders and A. W. Thomas, Report No. TH3443-CERN, 1982 (unpublished).
[15]A. S. Carroll *et al.*, Phys. Rev. Lett. 41, 777 (1978).
[16]R. P. Bickerstaff and B. G. Wybourne, J. Phys. G 7, 275 (1981); 7, 995(E) (1981).
[17]We thank Dr. D. J. Millener for supplying us with an independent derivation of Eq. (2.6).
[18]Equation (2.6) can also be obtained by exploiting the permutation symmetry of the $Q^6$ wave function; see S. Schindler and R. Mirman, J. Math. Phys. 18, 1678 (1977); 18, 1697 (1977); D. Strottman, *ibid.* 20, 1643 (1979).
[19]M. M. Nagels, T. A. Rijken, and J. J. de Swart, Phys. Rev. D 15, 2547 (1977); 20, 1633 (1979).
[20]M. Bozoian, J. C. H. van Doremalen, and H. J. Weber, Phys. Lett. 122B, 138 (1983).
[21]R. L. Jaffe and F. E. Low, Phys. Rev. D 19, 2105 (1979).
[22]A. M. Badalyan and Yu. A. Simonov, in *Proceedings of the International Conference on Hypernuclear and Kaon Physics, Heidelberg, Germany, 1982* (Max-Planck-Institut für Kernphysik, Heidelberg, 1982), p. 281; M. Soldate (unpublished). The existence of Soldate's work was kindly pointed out to the authors by R. L. Jaffe.
[23]H. Pilkuhn, *The Interactions of Hadrons* (North-Holland, Amsterdam, 1967), Chaps. 1 and 2.
[24]C. B. Dover and A. Gal, Ann. Phys. (N.Y.) 146, 309 (1983); C. B. Dover, Nukleonika 25, 521 (1980).
[25]P. M. Dauber *et al.*, Phys. Rev. 179, 1262 (1969).
[26]J. P. Berge *et al.*, Phys. Rev. 147, 945 (1966).
[27]G. Burgun *et al.*, Nucl. Phys. B8, 447 (1968).
[28]J. S. McCarthy, I. Sick, and R. R. Whitney, Phys. Rev. C 15, 1396 (1977).
[29]F. C. Khanna, Nucl. Phys. A165, 475 (1971).
[30]H. W. Fearing, Phys. Rev. C 16, 1313 (1977).
[31]A. T. M. Aerts and C. B. Dover, Phys. Rev. Lett. 49, 1752 (1982).
[32]V. Flaminio *et al.*, Report No. CERN-HERA 79-02, 1979 (unpublished).
[33]G. P. Gopal *et al.*, Nucl. Phys. B119, 362 (1977).
[34]P. M. Dauber *et al.*, Phys. Lett. 23, 154 (1966).
[35]D. O. Huwe, Phys. Rev. 181, 1824 (1969).